Nanostructure in Fe0.65Cr0.35 close to the upper limit of the miscibility gap

Alexander Dahlström, Frederic Danoix, Peter Hedström, Joakim Odqvist, Helena Zapolsky

Nanostructure in Fe0.65Cr0.35 close to the upper limit of the miscibility gap

Alexander Dahlström[a,b,*], Frederic Danoix[a], Peter Hedström[b], Joakim Odqvist[b], Helena Zapolsky[a]

[a] University of Rouen Normandie, INSA Rouen, CNRS, Groupe de Physique des Matériaux, 76000 Rouen, France
[b] Department of Materials Science and Engineering, KTH (Royal Institute of Technology), SE-100 44 Stockholm, Sweden

ARTICLE INFO

Article history:
Received 1 November 2019
Revised 14 January 2020
Accepted 19 January 2020

Keywords:
Phase separation
Atom probe tomography
Atomistic modelling
Stainless steel

ABSTRACT

The nanostructure of an Fe0.65Cr0.35 alloy has been investigated by atom probe tomography after high-precision thermal treatments close to the upper limit of the miscibility gap (MG). It is found that the wavelength of the decomposed ferrite between Cr- and Fe-rich regions grows exponentially when approaching the upper limit of the MG. Furthermore, the nanostructure change is gradual with temperature indicating a narrow metastable region and a diffuse transition out of the spinodal regime. Atomistic modelling near the limit of instability further supports the experimental observations. The findings are discussed in relation to the Cahn-Hilliard theory.

Stainless steels are versatile alloys used in, for example, energy industry [1,2]. Their attractive properties include a combination of high strength and excellent resistance towards corrosion. FeCr is the base alloy system for stainless steels, where Cr contributes to the "stainlessness". However, demixing of Fe and Cr is known to cause significant degradation of the toughness [3–5]. This is a potential issue for all FeCr based alloys that contain either the BCC or the BCT phase. Hence, phase separation when α decompose into α (Fe-rich) + α'(Cr-rich) is important to consider in technical applications [6–9]. The mechanism through which phase separation occurs is, at an early kinetic stage, either nucleation and growth (NG) or spinodal decomposition (SD). Whereas the later stage of kinetics in both cases can be described by coarsening theory [10]. The limit of the unstable spinodal regime is often defined by the concentration (C) dependant Gibbs energy (G) locus at: $\partial^2 G/\partial C^2 = 0$. However, it is known from experiments that a gradual transition zone may better describe the spinodal limit [11,12]. This aspect has also been treated theoretically [13,14]. The Cahn-Hilliard (CH) equation is frequently used to model SD in FeCr by the temporal evolution of Cr compositional fluctuations [3,15–17]. In the FeCr case, the CH equation can be described by G and a gradient energy term (K), i.e. neglecting the α/α' coherency strain. The maximum amplification factor in the CH theory relates to the maximum velocity wavelength (λ_m) of the developing structure. λ_m can be related to the critical wavelength (λ_c) by $\lambda_m = \sqrt{2}\lambda_c$, where the critical wavelength is given by $\lambda_c = \sqrt{2K/(-\partial^2 G/\partial C^2)}$ [18]. In the early stages of phase separation before α/α'equilibrium volume fraction has been established α'coarsening is here neglected. It is also assumed in this work that the measured mean wavelength, λ, in the early stages has been developed at maximum velocity (i.e. λ_m). When the spinodal limit is approached, the wavelength λ_c is predicted to go towards infinity because $\partial^2 G/\partial C^2 \to 0$ [19]. Therefore, λ_c of SD varies across the MG depending on $\partial^2 G/\partial C^2$ [11]. However, it is cumbersome to accurately model SD and its periodic length-scale in the FeCr system using CH, in part due to the complexity of the concentration dependant gradient energy term K [20,21] and the effect of the initial nanostructure on the kinetics of SD [22,23]. To further explore the varying nanostructure at different temperatures within the MG we here study the nanostructural changes as the critical upper temperature limit (T_c) of the MG is approached in an $Fe_{0.65}Cr_{0.35}$ alloy. The experiments are conducted by highly precise thermal treatments and atom probe tomography (APT) analyses. To supplement the experimental observations Khachaturyan's atomic density function theory is used [24]. Based on this theory, the temporal evolution of the system is modelled through minimisation of the free energy given by the difference in chemical potential without explicitly stating K in the energy function.

The $Fe_{0.65}Cr_{0.35}$ alloy was supplied by the company OCAS N.V. with the realised composition Fe–34.61Cr–0.04Al–0.0016C in at %.

* Corresponding author at: Department of Materials Science and Engineering, KTH (Royal Institute of Technology), SE-100 44 Stockholm, Sweden.
E-mail address: adahlstr@kth.se (A. Dahlström).

https://doi.org/10.1016/j.scriptamat.2020.01.024

Table 1
The ΔHV (i.e. HV change after ageing relative to the solution treated state), variation V, and wavelength λ *(from APT)* all after 120 hrs of ageing.

Temperature	ΔHV	V	λ[nm]
as-quenched	0.0 ± 3.5	0.02	–
550 °C	147.9 ± 12.1	1.05	10.8
560 °C	138.8 ± 19.9	1.00	11.0
563 °C	39.3 ± 12.4	0.49	13.2
565 °C	56.8 ± 6.9	–	–
567 °C	29.3 ± 4.0	–	–
568 °C	35.4 ± 7.5	0.43	20.4
569 °C	−1.3 ± 7.5	–	–
570 °C	−22.8 ± 8.2	0.19	–
580 °C	−16.8 ± 9.0	–	–

The following solution treatment of 0.3×10×15 mm sheets was conducted: 2 h at 1100 °C before water quenching and subsequent thermal ageing in a JOFRA 601 calibration furnace, with a temperature accuracy of ±0.9 °C. APT needles were prepared using the classical two-step electro-polishing method using a microloop [25]. A local electrode APT system LEAP 4000HR from CAMECA® was used, with the operating parameters: 50 K, pulse fraction 20% and detection rate 0.2%. The reconstruction parameters were optimised in IVAS 3.6.8 using spatial distribution maps [26,27]. The LEAP system allows for a large field-of-view which means a higher probability of detecting crystallographic features such as the <011>-Fe pole with low impact density [28]. Using such crystallographic features the interatomic plane distance was corrected in accordance with the reconstruction procedure as suggested by Moody et al. [26]. Quantification of the mean wavelength was based on autocorrelation function along the analysis axis for optimal resolution. The autocorrelation analysis in this work allowed for a maximum λ of 120 nm. Statistical frequency distribution (Freq. Dist.) analyses were performed in representative volumes of ~1million ions excluding the low index pole regions, as in Moody et al. [29]. In this work, the Freq.Dist. bin volume was 50 ions collected at a detection efficiency of 36%. In addition, the variation parameter (V) defined by Blavette et al. [30] utilising Freq.Dist. was used to quantify the extent of demixing based on relative Cr amplitudes.

The results from Vickers micro-hardness ($HV_{0.2}$) measurements of these samples are presented in Table 1. 15 measurements were conducted in accordance with the ISO 6507-1 standard. The reported value is the mean out of 11 measurements after excluding the four extreme values, the uncertainty is given by the standard deviation. The samples were aged 120 h at temperatures from 550 °C and higher. The 120 h was selected after prior kinetic HV investigation at 525 °C that showed a steady HV evolution after 120 h [31].

Table 1 shows larger ΔHV at lower temperatures, i.e. at greater driving force by deeper undercooling from the limit of the MG which favour SD. It should be noted that ΔHV is known to be related to the amplitude of Cr fluctuations in the sample through V [32]. In the range 563–568 °C, ΔHV is lower but fairly constant, while at higher temperatures ΔHV is negative. The negative values may be an effect of some recovery of the alloys. Based on these hardness results, samples aged at 550, 560, 563, 568 and 570 °C were selected for further APT analyses. APT 2D Cr composition cross sections obtained with the gpm3Dsoft software developed at the University of Rouen, are displayed in Fig. 1 [33].

Considering the minor temperature difference (i.e. negligible effects on Cr diffusion), the evolution of nanostructure is most likely a thermodynamic effect of approaching the spinodal and/or the limit of the MG. Since the driving force of α' formation should decrease at higher temperature, this can be seen quantitatively by the decrease of V. The Cr composition distribution maps are shown in volumes of 10×30×90 nm, for direct visual comparison of λ. Furthermore, the influence of temperature on nanostructure can be observed in 3D by evaluating α/α' Cr composition fluctuations based on proxigrams in the normal direction of the nominal composition *iso*-surface [34]. An interconnected SD structure associated with Fe/Cr phase separation can easily be detected at 560 °C, 563 °C and 568 °C. But there is no interconnected SD structure nor α' precipitates at 570 °C. Nevertheless, there exist small Cr fluctuations around the nominal composition which are quantitatively significant relative to the as-quenched state (i.e. $V = 0.19$ versus $V = 0.02$ in Table 1). For the $Fe_{0.65}Cr_{0.35}$ alloys no distinction could be made between the metastable binodal and the unstable spinodal regimes within the MG. This supports the view of a very narrow metastable region near T_c (if it exists), and consequently the transition zone over T_c appears "diffuse". It should be emphasised that whether the spinodal curve coexists with the limits of the MG at $Fe_{0.65}Cr_{0.35}$ is not concluded here. The abrupt change in morphology is thus an effect of driving force and hence indicative of approaching the MG limit. The result is shown in Fig. 3 and presented in Table 1.

To supplement the experimental results, atomistic modelling was performed using a quasiparticle approach proposed by Lavrskyi et al. [36], which is based on Khachaturyan's theory [24]. In the quasiparticle approach, the size of the simulation grid is smaller than the interatomic distance. Thus, atoms will occupy a spherical volume containing some number of simulation grid points. Hence, simulation grid points inside of atomic spheres are regarded as atomic fragments and referred to as Fratons. The main variable of the simulation is the occupation probability function $\rho_A(\vec{r})$ which is the probability that a Fraton of the sort A, situated at point *r*, is inside of any atomic sphere at moment *t*. The proper choice of a model Hamiltonian requires describing the interaction of Fratons that should result in both their "condensation" into atomic spheres and the movement of the spheres into the desired atomic equilibrium configuration, all driven by the spontaneous minimisation of the free energy. The model potential of this Hamiltonian contains short-range and long-range interactions. The short-range interaction is chosen as a step function where the negative part defines the atomic radius, and the positive part assures the repulsion of atomic spheres at short distance. For the BCC structure, the long-range AA and BB Fraton interactions are fitted by a one mode potential chosen as a Gaussian function with the minima centred at the first neighbour distance of the BCC lattice. The width of the Gaussian functions defines the elastic properties of the system, and in this case, the BCC-Fe elastic constants were fitted to the DFT calculations by Mendelev et al. [35]. The Helmholtz energy of the system *F*=*U*-TS is written in mean-field approximation, where the first term describes the internal energy of the system and the second term is related to entropy. The temporal evolution of the density function of Fratons $\rho_A(\vec{r})$ can be written using the kinetic Landau-Khalatnikov equation [31] governed by the minimisation of Helmoltz energy:

$$\frac{d\rho_A(\vec{r},t)}{dt} = \sum_{r'}\sum_{B=1}^{B=m}\frac{L_{AB}(\vec{r}-\vec{r}')}{k_BT}\frac{\delta F}{\delta\rho_B(\vec{r}',t)}$$

Where, m is the number of components, k_B is the Boltzmann constant, T is temperature and $L_{AB}(\mathbf{r})$ is a matrix of kinetic coefficients related to the probabilities of elemental diffusional jumps from lattice site r to r' on a Bravais lattice during a time unit. The $\rho_A(\vec{r})$ is a conserved variable and in the case of a binary system to describe the atomic configuration only one $\rho_A(\vec{r})$ function is needed. In this work, we simulate the BCC-Fe equilibrium structure (i.e. $\bar{\rho}_A$) and then introduce a second substitutional component $\bar{\rho}_B$. To describe phase separation kinetics, the long-range AB potential is chosen as a Gaussian function centred at $k = 0 : V_{AB} = -\mu \cdot \exp(-k^2/2\sigma^2)$. Here, a dimension coefficient μ defines the strength

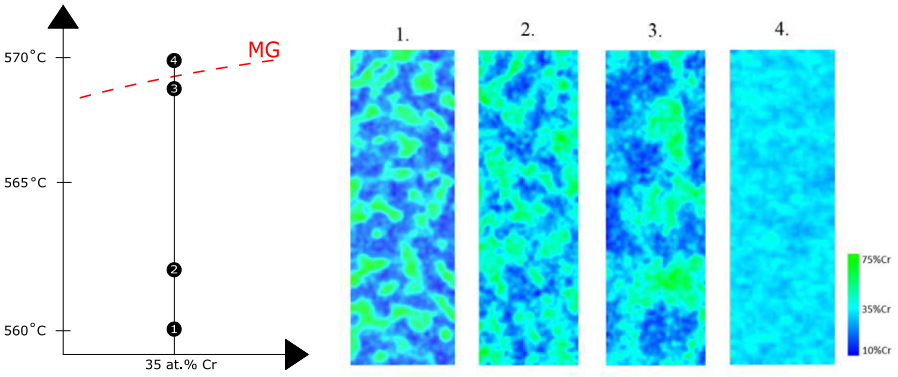

Fig. 1. APT results of the nanostructure at increasing temperatures close to the limit of the MG, 2D Cr composition maps from 10×30×90 nm, wavelengths from autocorrelation. 1.) 560 °C, λ = 11 nm, 2.) 563 °C, λ = 12 nm, 3.) 568 °C, λ = 20 nm, 4.) 570 °C no λ can be evaluated. The suggested limit of the MG (i.e. T_c) lies in-between 3. and 4. indicated by the dotted red line. (For interpretation of the references to colour in this figure legend, the reader is referred to the web version of this article.)

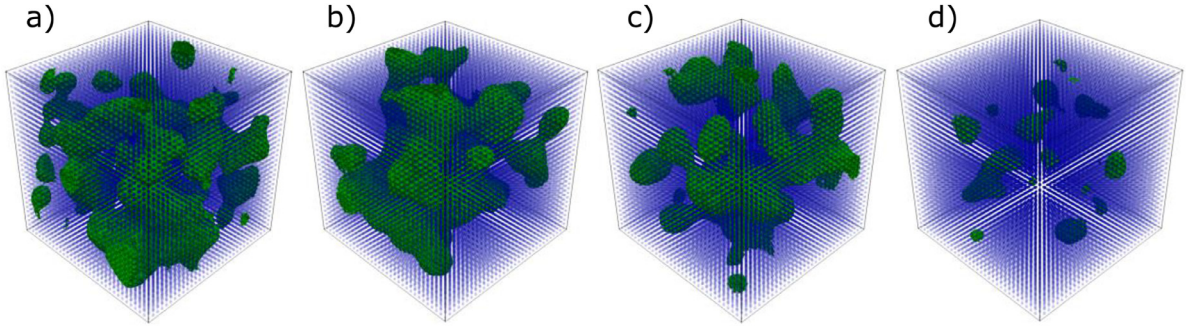

Fig. 2. Simulated microstructure at different temperatures in the A(blue)–35B(green) system using the quasiparticle approach at $t^* = 2{\cdot}10^6$. Temperatures: a) 565 °C, b) 567 °C, c) 568 °C, d) 572 °C. The parameters of these simulations are: volume $256\Delta x^3$, lattice parameter a_0=8Δx, $\bar{\rho}_A = 0.1232$, $\bar{\rho}_B = 0.0017$. (For interpretation of the references to colour in this figure legend, the reader is referred to the web version of this article.)

of the interaction A/B. Thus, μ impacts the driving force of separation kinetics, and, consequently, the simulation time to observe the wavelength λ. In this work, a good compromise between simulation and real-time was found with μ=0.08, SD has been modelled by quasiparticles using the same reduced system variables as by Lavrskyi et al. [36]. Spinodal decomposition is simulated as isothermal "ageing" below the spinodal line with an initially homogeneous but disordered solid solution. The driving force of phase separation, i.e. temperature is adjusted by the negative depth of the long-range potential. Thus, zero driving force (i.e. $\partial^2 G/\partial C^2 = 0$) is set as equivalent to T_c to serve as a reference point for the experimental comparison [31,36].The as-quenched state of the system is determined by an initial condition: $\rho_i(r, t = 0) = \bar{\rho}_i + \delta\rho_i(r)$ ($i = A$ or B) where $\bar{\rho}_i$ is the average density of the component i and $\delta\rho_i(r)$ are small perturbations generated by a random number generator. To perform the simulations a semi-implicit Fourier spectral method was used to solve the kinetic equation in reciprocal space [37]. Thus, the matrix of kinetic coefficients in reciprocal space can be written as: $L_{AB}(k) = -L^0_{AB}k^2$ where L^0_{AB} is the jump probability between A and B Fratons at nearest-neighbour sites at a time unit. In particular, we chose $L^0_{AA} = L^0_{BB} = 1$ and $L^0_{BA} = L^0_{AB} = -0.5$.

Fig. 2 shows the simulated microstructure of the A-35B alloy at time t^*=$2{\cdot}10^6$, aged at different temperatures. In our simulations, the critical temperature of instability was defined as the limit observed in the experiments as T_c. Hence, at temperatures $T/T_c < 1$ the decomposed microstructure is observed.

To evaluate the spinodal structure from modelling results at different temperatures, the structure factor $S(\boldsymbol{k})$ was calculated directly from the atomic distributions in reciprocal space. The evolution of the calculated $S(\boldsymbol{k})$ as a function of temperature is presented in Fig. 3b). In the simulations $S(\boldsymbol{k})$ decrease rapidly approaching the limit of instability, as $S(\boldsymbol{k})$ is calculated in reciprocal space, the inverse trend is true for λ in real space. Thus, this trend agrees well with our APT observations.

Our experiments and simulations suggest a rapid increase of λ as T_c and the spinodal is approached. The decrease in the extent of Cr compositional fluctuations given by V suggests that there is no distinct difference in mechanism of phase separation and that the spinodal limit is close to the limit of the MG. However, quantitatively at 570 °C, the Fe–35Cr sample is far from homogeneous. Short-range clustering due to the high Cr–Cr affinity has previously been seen to be temperature-dependant even at high temperature in Fe–Cr [23], with increasing intensity closer to the limit of the MG [22].

The point to highlight from the APT analyses in Fig. 3a) is that even though it is not possible to measure a characteristic wavelength at 570 °C, the decreasing trend of the V parameter continues. However, the value $V = 0.19$ obtained at 570 °C is almost 10 times greater than in the solution treated state (see Table 1). This might be a short-range clustering effect due to the proximity to the MG. It is possible to observe an exponential increase of λ in FeCr when the driving force goes towards zero, this rapid evolution of the structure is in agreement with CH, but it should be kept in mind that the theory only considers SD. In this work, the rapidly increasing trend starts very close to the suggested T_c at approximately $T/T_c = 0.98$ (i.e. ~560°C), which is why the high precision thermal treatments have been key to this study.

The periodicity of the spinodal structure is highly temperature-dependant within the MG, where λ classically decreases linearly with increasing driving force [13]. Prior works have questioned the formation of a λ_c near the spinodal curve, and thus the existence of an exact boundary near the instability locus [11,14]. Furthermore, the SD regime is more accurately defined as a region where the activation energy for phase separation becomes smaller than

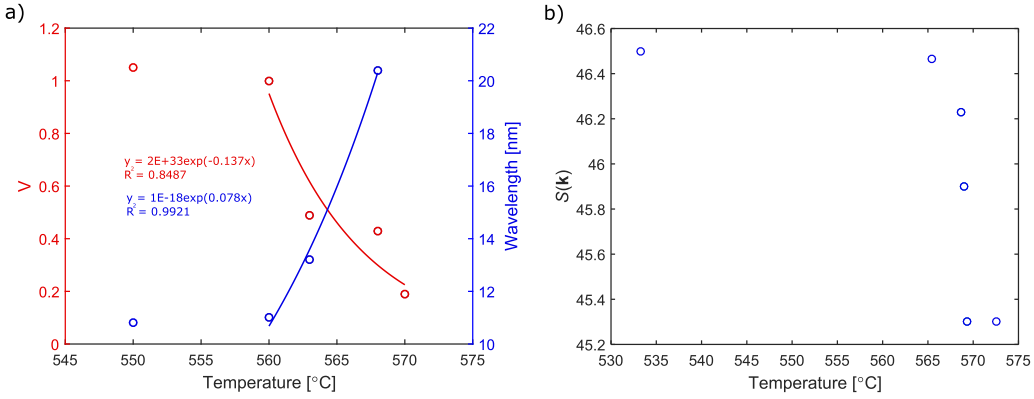

Fig. 3. a) The V-parameter from APT Freq.Dist analysis and λ from autocorrelation. When T_c is approached λ increase exponentially, the opposite trend is observed for V. b) The maximum of the calculated structure factor $S(k)$ from simulation results showing a rapid decrease in reciprocal space.

for thermal fluctuations [11]. Cr–Cr clustering may also exist to quantifiable extent due to short-range order effects outside of the MG in α without forming α' [38]. Considering low temperature composition dependant transition from SD to NG, a percolated α' structure makes discrimination between NG/SD experimentally cumbersome [39]. In addition during long-term heat treatment, linear approximation is generally deemed non-sufficient to describe later stages of low-temperature phase separation [40]. Instead, the LBM method which considers nonlinear diffusion is often used to describe the later stages of SD near-equilibrium [41]. This is all in support of a gradual/diffuse transition out of the SD regime where we can experimentally measure an exponential increase of λ in the range 0.98–0.998T/T_c (i.e. up until 1°C below T_c).

In summary, these direct observations of the λ evolution close to the limit of the Fe–35Cr MG in 3D by APT, confirmed by simulation results, are novel of their kind. Considering the incremental temperature differences, this effect is most likely due to the difference in driving force when undercooling below the limit of the MG.

Declaration of Competing Interest

The authors declare that they have no known competing financial interests or personal relationships that could have appeared to influence the work reported in this paper.

Acknowledgement

The financial support from Centre National de la Recherche Scientifique (CNRS), Region-Normandie and Carl Tryggers Research Foundation is gratefully acknowledged. Supercomputing capability at Centre Régional Informatique et d'Applications Numériques de Normandie (CRIANN) is also acknowledged. This work was partly carried out owing to the experimental GENESIS platform. GENESIS is supported by the region Haute Normandie, the Metropole Rouen Normandie, the CNRS via LABEX EMC and the French National Research Agency as part of the program "Investissement d'avenir" ARN-11-EQPX-0020.

References

[1] K.H. Lo, C.H. Shek, J.K.L. Lai, Mater. Sci. Eng. R: Rep. 65 (2009) 39–104.
[2] C. Capdevila, J. Chao, J.A. Jimenez, M.K. Miller, Mater. Sci. Technol. 29 (2013) 1179–1184.
[3] O. Soriano-Vargas, E.O. Avila-Davila, V.M. Lopez-Hirata, N. Cayetano-Castro, J.L. Gonzalez-Velazquez, Mater. Sci. Eng. A 527 (2010) 2910–2914.
[4] C. Capdevila, M.K. Miller, I. Toda, J. Chao, Mater. Sci. Eng. A 527 (2010) 7931–7938.
[5] A. Pineau, J. Besson, in: Duplex Stainless Steels, John Wiley & Sons, Ltd, 2013, pp. 161–208.
[6] C. Capdevila, M.K. Miller, J. Chao, Acta Mater. 60 (2012) 4673–4684.
[7] J. Wallenius, P. Olsson, L. Malerba, D. Terentyev, Nucl. Instrum. Methods Phys. Res. Sect. B Beam Interact. Mater. At. 255 (2007) 68–74.
[8] K.L. Wong, H.-J. Lee, J.-H. Shim, B. Sadigh, B.D. Wirth, J. Nucl. Mater. 386–388 (2009) 227–230.
[9] D. Terentyev, L. Malerba, A. v. Barashev, Philos. Mag. Lett. 85 (2005) 587–594.
[10] Z. Yan, Y. Li, X. Zhou, Y. Zhang, R. Hu, J. Alloys Compd. 725 (2017) 1035–1043.
[11] K. Binder, C. Billotet, P. Mirold, Z. Phys. B Condens. Matter 30 (1978) 183–195.
[12] W. Xiong, M. Selleby, Q. Chen, J. Odqvist, Y. Du, Crit. Rev. Solid State Mater. Sci. 35 (2010) 125–152.
[13] E.L. Huston, J.W. Cahn, J.E. Hilliard, Acta Metall. 14 (1966) 1053–1062.
[14] J.W. Cahn, J.E. Hilliard, J. Chem. Phys. 31 (1959) 688–699.
[15] J.W. Cahn, Acta Metall. 9 (1961) 795–801.
[16] Y.-S. Li, H. Zhu, L. Zhang, X.-L. Cheng, J. Nucl. Mater. 429 (2012) 13–18.
[17] T. Barkar, L. Höglund, J. Odqvist, J. Ågren, Comput. Mater. Sci. 143 (2018) 446–453.
[18] J.W. Cahn, J. Chem. Phys. 42 (1965) 93–99.
[19] J.W. Cahn, J.E. Hilliard, J. Chem. Phys. 28 (1958) 258–267.
[20] J.M. Hyde, A.P. Sutton, J.R.G. Harris, A. Cerezo, A. Gardiner, Model. Simul. Mater. Sci. Eng. 4 (1996) 33.
[21] A. Cerezo, J.M. Hyde, M.K. Miller, S.C. Petts, R.P. Setna, G.D.W. Smith, Philos. Trans. R. Soc. Lond. Ser. Phys. Eng. Sci. 341 (1992) 313–326.
[22] X. Xu, J. Odqvist, M.H. Colliander, S. King, M. Thuvander, A. Steuwer, P. Hedström, Acta Mater. 134 (2017) 221–229.
[23] J. Zhou, J. Odqvist, L. Höglund, M. Thuvander, T. Barkar, P. Hedström, Scr. Mater. 75 (2014) 62–65.
[24] A.G. Khachaturyan, Theory of Structural Transformations in Solids, Wiley, New York, 1983.
[25] M.K. Miller, R.G. Forbes, Atom-Probe Tomography, Springer U.S., Boston, M.A., 2014.
[26] M.P. Moody, B. Gault, L.T. Stephenson, D. Haley, S.P. Ringer, Ultramicroscopy 109 (2009) 815–824.
[27] F. Vurpillot, M. Gruber, G. Da Costa, I. Martin, L. Renaud, A. Bostel, Ultramicroscopy 111 (2011) 1286–1294.
[28] B. Gault, F. Danoix, K. Hoummada, D. Mangelinck, H. Leitner, Ultramicroscopy 113 (2012) 182–191.
[29] M.P. Moody, L.T. Stephenson, A.V. Ceguerra, S.P. Ringer, Microsc. Res. Tech. 71 (2008) 542–550.
[30] D. Blavette, G. Grancher, A. Bostel, J. Phys. Colloq. 49 (1988) C6-433–C6-438.
[31] A. Dahlström, Influence of a Mechanical Load on the Ageing of Fe-Cr Alloys Ph.D. thesis, Normandie Université, 2019.
[32] F. Danoix, P. Auger, Mater. Charact. 44 (2000) 177–201.
[33] W. Lefebvre-Ulrikson, F. Vurpillot, X. Sauvage, Atom Probe Tomography Put Theory Into Practice, 2016.
[34] O.C. Hellman, J.A. Vandenbroucke, J. Rüsing, D. Isheim, D.N. Seidman, Microsc. Microanal. 6 (2000) 437–444.
[35] M.I. Mendelev, S. Han, D.J. Srolovitz, G.J. Ackland, D.Y. Sun, M. Asta, Philos. Mag. 83 (2003) 3977–3994.
[36] M. Lavrskyi, H. Zapolsky, A.G. Khachaturyan, ArXiv:14115587 Cond-Mat (2014).
[37] L.Q. Chen, J. Shen, Comput. Phys. Commun. 108 (1998) 147–158.
[38] H. Kuwano, Trans. Jpn. Inst. Met. 26 (1985) 473–481.
[39] W. Xiong, P. Hedström, M. Selleby, J. Odqvist, M. Thuvander, Q. Chen, Calphad 35 (2011) 355–366.
[40] K. Binder, P. Fratzl, Wiley-VCH Verlag GmbH & Co. KGaA, 2001, pp. 409–480.
[41] T. Ujihara, K. Osamura, Mater. Sci. Eng. A 312 (2001) 128–135.